IRAQI JOURNAL OF APPLIED PHYSICS
Vol. 22, No. 4, October-December 2026, pp. 623-629

**Rajaa H. Farhan***
**Jamal F. Mohammed**

Department of Physics,
College of Education for
Pure Sciences,
University of Anbar,
Ramadi, IRAQ
* Corresponding author email:
raj24u3003@uoanbar.edu.iq


# Enhanced Room-Temperature $NO_2$ Gas Detection of ZnO/$SnO_2$/CdS Multilayer Heterostructure

The trilayer, ZnO/$SnO_2$/CdS heterostructure was deposited on p-type silicon (p-Si) substrate by spray pyrolysis for application in $NO_2$ gas sensing. The phase of three components polycrystalline including ZnO, $SnO_2$ and CdS was confirmed with average crystallite size of 14.14 nm and a microstrain of $3.14\times10^{-3}$ reflecting high defect density and high number of active sites on surface. A uniform nanostructured morphology to increase the effective surface area was also confirmed. The UV-visible absorption and low energy band gap of 2.5 eV are indicative of interfacial effects in the multilayer system. Gas sensing tests toward 75 ppm $NO_2$ demonstrated a maximum sensitivity of 26% at room temperature (25°C), with fast response and recovery behavior. The enhanced performance at room temperature is attributed to crystallite size-induced depletion effects and defect-assisted charge transfer across the heterointerfaces. These results indicate that the ZnO/$SnO_2$/CdS/p-Si heterostructure is a promising candidate for room-temperature $NO_2$ detection.

**Keywords:** Heterostructures; Spray pyrolysis; Gas sensors; Multilayer thin films
Received: 7 March 2026; Revised: 5 May 2026; Accepted: 12 May 2026; Published: 1 October 2026

## 1. Introduction

Nitrogen dioxide ($NO_2$) is one of the most hazardous air pollutants produced from industrial activities, combustion engines, and fossil fuel consumption. Even at low concentrations, $NO_2$ poses serious risks to human health and contributes to environmental issues such as acid rain and photochemical smog. Therefore, the development of sensitive, low-cost, and room-temperature gas sensors for $NO_2$ detection has attracted significant research interest in recent years [1,2].

Semiconducting metal oxides such as zinc oxide (ZnO) and tin oxide ($SnO_2$) are widely used in gas sensing applications due to their high chemical stability, wide band gap, and strong surface reactivity. In practice, their sensing mechanism is mainly related to the surface adsorption desorption processes and the modulation of depletion layer near the surface. Nonetheless, traditional single-layer oxide sensors also need to be operated at higher temperatures to reach satisfactory sensitivity [3], resulting in more power consuming and limiting practical applications.

In order to address these shortcomings while maintaining the benefits of two dimensional materials, multilayer heterostructures have been developed as a promising but largely unexplored approach to achieving improved gas sensing performance. Heterojunctions between various semiconductors can generate internal electric fields; tune EF and Ec by modifying band arrangement; facilitate charge transfer at the heterointerfaces. This effects results in better control of the potential barrier at grain boundaries and higher resistance change when the gas molecules are adsorbed on their surfaces. Specifically, the introduction of a narrow band gap semiconductor, including that of cadmium sulfide (CdS), in connection with wide band gap oxides such as ZnO and $SnO_2$ serves to extend optical absorption and affect charge distribution at the interface [4].

Moreover, decreasing the crystallite size down to the nanometer scale increases the surface-to-volume ratio and enhances the number of active sites contributing to gas adsorption. Additional contributions to the formation of adsorption centers and charge exchange processes are generated by microstrain and lattice defects. At the same time, as the grain increase in size approaches the depletion width, the entire crystal or grain will be readily active to surface reactions and may thus lead to an enhancement in response of the material to a gaseous analyte species at room temperature [5].

A multilayer ZnO/$SnO_2$/CdS heterostructure was deposited on p-Si substrate for the first time in this work by the spray pyrolysis technique. The films were characterized systematically with X-ray diffraction (XRD), field-emission scanning electron microscopy (FE-SEM), atomic force microscopy (AFM), and UV-visible spectrophotometry to study their structural, morphological, and optical properties. The gas sensing characteristic features of 75 ppm $NO_2$ regulating in different operating temperature range (25–200°C). The effect of crystallite size, and microstrain, and the role of multilayer interfaces upon the sensing mechanism is explained. The results proved that the designed heterostructure enhances its room-temperature $NO_2$ sensing performance, which brings potential value and new opportunities for low-temperature gas sensing.

## 2. Experimental Part

Figure (1) shows a schematic diagram representing the overall experimental procedure including substrate preparation, spray deposition, characterization

  

techniques, and gas sensing setup. Glass substrates ($2.5\times2.5cm^2$) were washed in a distilled water, sonicated in acetone, rinsed with ethanol, dried and weighed for determination of thickness of the substrate. Precursor solutions of ZnO $SnO_2$ and CdS were prepared by calculating molar concentrations, stirring them magnetically at 40°C for 30 min to uniform the solution and were filtered before deposition.

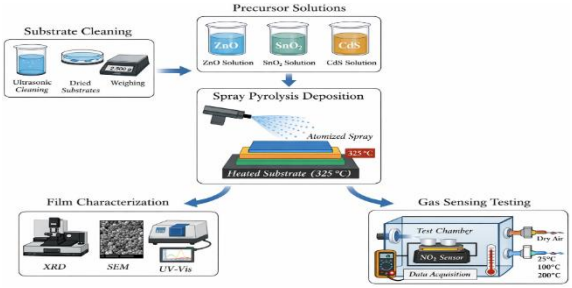


**Fig. (1) Schematic diagram of the fabrication of the fabricated $ZnO/SnO_2/CdS$ multilayer thin films by spray pyrolysis and their characterization and $NO_2$ gas sensing setup**

Spray pyrolysis technique was used for the deposition of thin films at 325°C substrate temperature, during the deposition process spray time was 5 s and pause between each spray of 25 s for complete thermal decomposition of droplets. First, layers were deposited on glass substrates, where layers were characterized in terms of structure and optics. Later multilayer of $ZnO/SnO_2/CdS$ films were sequentially deposited onto p-type silicon (p-Si) substrates with excess condition. The final thickness of the multilayer structure was ~350 nm. The structural properties were studied through the XRD for phase composition, crystallite size, and microstrain determination. The surface morphology was investigated by the FE-SEM and AFM. UV-visible spectrophotometry was used to analyze optical properties and Tauc's method was used for determining optical band gap. Temperature controlled chamber was used to perform gas sensing measurement toward 75 ppm $NO_2$ targeting operating temperatures 25°C, 100°C, and 200°C. During gas exposure and recovery cycles, the resistance of the sensor was evaluated and sensitivity was determined as resistance variation between gas and dry air. Using 90% criteria for response and recovery times. For gas sensing measurements, electrical contacts were applied on the top surface of the $ZnO/SnO_2/CdS$ multilayer film in a planar configuration. This arrangement ensures that the current flows laterally through the sensing film rather than through the p-Si substrate. The p-Si substrate primarily serves as a mechanical support. Nevertheless, the formation of a p-Si/n-type oxide heterojunction at the interface may introduce an additional potential barrier, which can influence charge distribution and slightly affect the overall sensing response. This configuration is commonly used in thin-film gas sensors to ensure film dominated conduction.

## 3. Results and Discussion

Figure (2) shows the XRD pattern of the $ZnO/SnO_2/CdS$ multilayer film deposited on a p-Si substrate. The diffraction peaks confirm the polycrystalline nature of the heterostructure, with reflections corresponding to hexagonal ZnO, tetragonal $SnO_2$, and hexagonal CdS phases. The peak located at $2\theta = 28.4°$ is attributed to the (111) plane of the silicon substrate. It is worth noting that the main diffraction peak of hexagonal CdS appears at approximately $2\theta = 26.5°$ corresponding to the (002) plane, which is sufficiently separated from the Si (111) peak. Therefore, no significant peak overlapping is expected in this region, and the phase identification remains reliable. The absence of additional impurity peaks further confirms the successful formation of the multilayer structure without secondary phases [6].

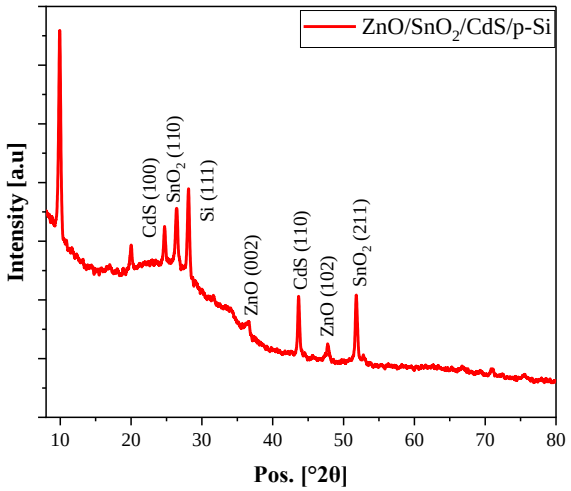


**Fig. (2) XRD pattern of the multilayer structure deposited on a silicon substrate**

The average crystallite size was estimated to be approximately 14.14 nm using the Scherrer's equation, indicating nanoscale crystallinity. The observed peak broadening arises from both finite crystallite size and lattice strain effects. The total broadening (β) can be expressed as a combination of size and strain contributions, where the strain-induced broadening is proportional to tanθ. By combining both effects, the relation $\beta=(k\lambda/D\cos\theta)+4\varepsilon\tan\theta$ is obtained. Rearrangement of this equation leads to $\beta\cos\theta=(k\lambda/D)+4\varepsilon\sin\theta$, which enables the separation of crystallite size and lattice strain contributions. Based on this formulation, the microstrain was estimated to be $3.14\times10^{-3}$, indicating the presence of lattice distortion and structural defects. Such nanoscale crystallite size combined with measurable lattice strain is expected to enhance surface reactivity and modify the surface charge distribution, which plays an important role in gas sensing performance.

Figure (3) shows the FE-SEM image of a

  

$ZnO/SnO_2/CdS$ multilayer thin film deposited on p-Si by spray pyrolysis. The surface shows an almost continuous granulated structure with homogeneously dispersed nanograins and without cracks and voids, which supports good continuity of the film and adhesion to the substrate. The average grain size was estimated to about 26 nm illustrating very clearly the nanoscale nature of desired layers deposited in each step. This small grain size indicates that this sequential layer may lead to control nucleation and growth. These lower layers probably serve as nucleation sites for later films preventing gross grain growth and promoting surface uniformity. Its compact and uniform morphology increases the gas-solid contact surface. The importance of such nanostructured surfaces is for gas sensing applications where such surfaces promote adsorption processes and improve charge transfer across grain boundaries.

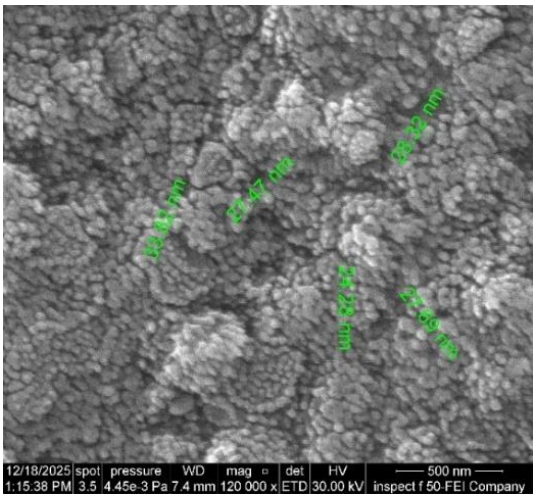


**Fig. (3) FE-SEM image of the multilayer sample deposited on a silicon substrate**

Figure (4) shows the AFM image of the $ZnO/SnO_2/CdS$ multilayer thin film deposited on p-Si. The surface shows an obvious granule and grain aggregation characteristics along the multilayer structure. In average the grain size from statistical analysis was around 141 nm, the value is greater than the crystallite size calculated from XRD analysis. The significant difference between the crystallite size (14 nm) obtained from XRD and the grain size (141 nm) observed from AFM indicates that each grain consists of multiple crystallites aggregated together. This aggregation leads to the formation of dense grain clusters. The apparent difference between the FE-SEM grain size (~26 nm) and the AFM-derived surface feature size (~141 nm) arises from the different nature of the two techniques. FE-SEM mainly resolves the lateral nanoscale grains on the film surface, whereas AFM records the three-dimensional surface topography and may include aggregated grain clusters, surface mounds, and tip-convolution effects. Therefore, the AFM value should be considered as an apparent surface feature size rather than the size of individual primary grains. In this sense, the XRD crystallite size (~14 nm), FE-SEM grain size (~26 nm), and AFM particle size (~141 nm) represent different structural length scales of the multilayer film. Cross-sectional SEM would provide further insight into the vertical growth morphology. Although such morphology reduce large-scale porosity, nanoscale intergranular pathways are still preserved, allowing gas diffusion through the film. Moreover, grain boundaries act as active sites for gas adsorption, which can enhance sensing performance.

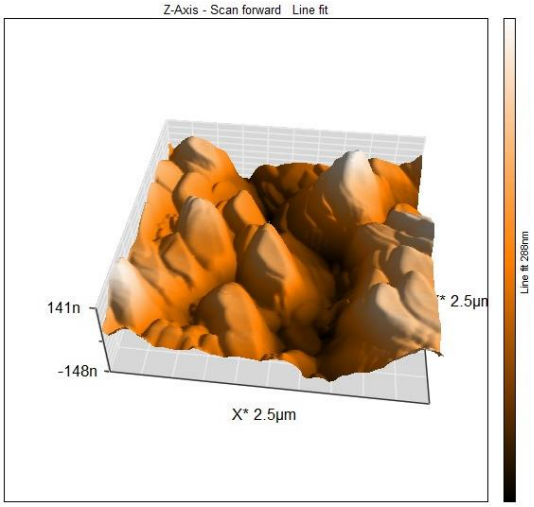


**Fig. (4) AFM image of $ZnO/SnO_2/CdS/P$-Si structure**

Figure (5) indicates the absorption spectrum of the multilayer $ZnO/SnO_2/CdS$ thin film structure. This structure exhibits strong absorption in the UV region with an absorption edge extending into the visible range. This behavior is primarily governed by the CdS layer due to its relatively narrow band gap. The absorption onset observed around 500-550 nm is consistent with the characteristic optical response of CdS [7]. In contrast, wide band gap oxides such as ZnO and $SnO_2$ mainly contribute to absorption in the ultraviolet region and have a limited influence in the visible range [6]. Therefore, the enhanced absorbance in the visible region can be mainly attributed to the presence of CdS rather than strong interfacial optical effects. Minor contributions from nanoscale features and defects may slightly influence the absorption edge, however, their role is considered secondary compared to the dominant effect of the CdS layer [8]. The decrease in absorbance at higher wavelengths is consistent with the behavior of semiconductors, where the photon energy becomes insufficient to promote electronic transitions across the band gap.

Figure (6) shows the variation of absorption coefficient (α) with wavelength for the multilayer $ZnO/SnO_2/CdS$ thin film structure. The absorption coefficient in the visible region is lower than the absorption coefficient in the UV region and are slowly

  

diminishing at longer wavelengths. Proper semiconducting behavior is highlighted by the fact that the threshold energy for photon absorption is of the order of the band gap so that in a wide range of photon energies there is little or no absorption up to a threshold energy followed by an enormous increase [9]. The higher absorption coefficient (α) values in short-wavelength region imply that efficient photon absorption occurs across a small penetration depth in the multilayer structure, verifying the strong light-matter interaction. In contrast, in nanostructured thin films higher absorption coefficients are correlated with better light-matter coupling, surface states and interfacial effect that increases transition probability [10]. The slow decrease of absorption coefficient (α) with wavelength (λ) is general and reflects the lower energy of the photons and the lower probability of allowed electronic transitions at these longs wavelengths.

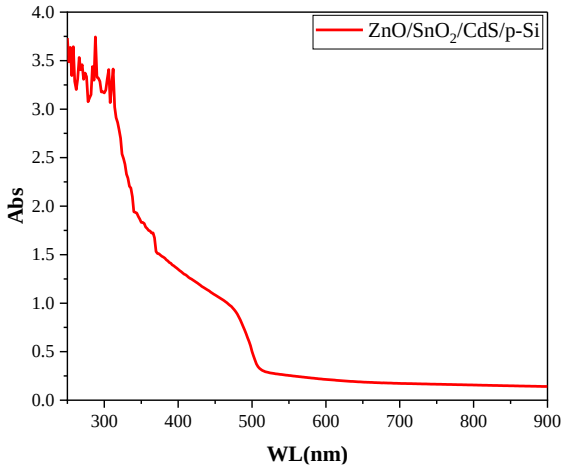


**Fig. (5) Absorption spectrum of the multilayer structure deposited on silicon**

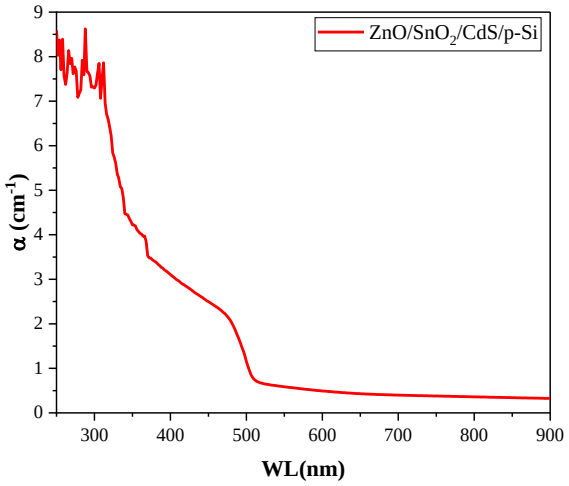


**Fig. (6) Variation of the absorption coefficient of the multilayer structure deposited on silicon with wavelength**

Figure (7) shows the optical band gap of the multilayer ZnO/$SnO_2$/CdS thin film, determined using Tauc's relation for direct allowed transitions. The extrapolation of the linear region of the $(\alpha h\nu)^2$ versus hν plot yielded an estimated band gap value of approximately 2.5 eV. This value is lower than that of wide band gap oxides such as ZnO (3.3 eV) and $SnO_2$ (3.6 eV), and is close to that of CdS (2.4 eV), indicating that the optical transition is primarily governed by the CdS layer within the multilayer structure [11]. This interpretation is consistent with the absorption edge observed in the visible region. Therefore, the contribution of ZnO and $SnO_2$ to the band gap determination in this measurement is considered limited, as their optical response is mainly confined to the ultraviolet region. Minor deviations from the bulk CdS band gap may be attributed to nanoscale effects such as crystallite size and structural imperfections, which can introduce slight band tailing (Urbach-type behavior) near the absorption edge [12].

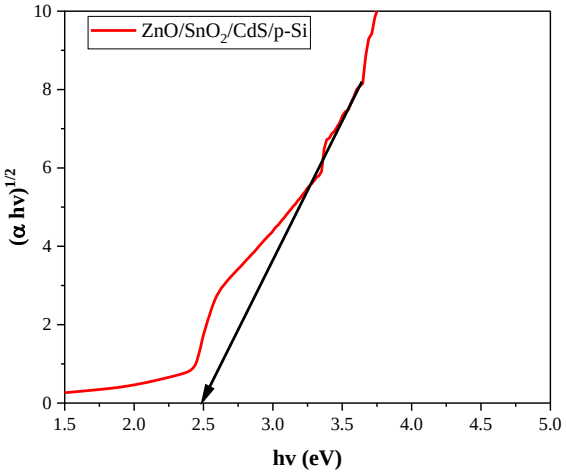


**Fig. (7) Determination of energy gap of the multilayer structure deposited on silicon**

Figure (8) shows the dynamic resistance response of the ZnO/$SnO_2$/CdS/p-Si sensor toward 75 ppm $NO_2$ at different operating temperatures. The highest resistance change is observed at room temperature (25°C), indicating effective modulation of charge transport under these conditions. This behavior is primarily governed by the presence of multiple heterojunctions formed at the ZnO/$SnO_2$, $SnO_2$/CdS, and CdS/p-Si interfaces [13]. Under air conditions, these interfaces create built-in potential barriers and depletion regions due to band alignment between the contacting semiconductors. These barriers restrict charge transport, resulting in a relatively high baseline resistance. Upon exposure to $NO_2$ gas, electrons are withdrawn from the n-type layers (ZnO and $SnO_2$) and the CdS layer, leading to an expansion of the depletion regions and an increase in the barrier height at each interface [14]. Because the multilayer structure behaves as a series of coupled heterojunctions, this barrier modulation results in an amplified resistance response.

At 100°C, although the same resistance increase

  

trend is observed, the overall resistance change decreases. This can be attributed to the increased contribution of thermally activated carriers, which reduce the baseline resistance and partially screen the effect of barrier modulation. At higher temperature (200°C), thermally activated desorption becomes dominant, limiting charge transfer at the surface and reducing the modulation of interfacial barriers, resulting in a further decrease in the sensing response [15].

The temperature-dependent sensing behavior is governed by the interplay between interfacial barrier modulation and adsorption-desorption kinetics. While nanoscale features and defect states provide active sites for gas adsorption and facilitate charge exchange, the dominant mechanism in the present multilayer system is the modulation of potential barriers across the heterojunction interfaces.

Figure (9) illustrates the response and recovery times of the ZnO/$SnO_2$/CdS/p-Si sensor to 75 ppm $NO_2$ at various temperature. The response time slightly improve as the temperature raise, while the recovery time decrease even more significantly with raising temperature. The fast response at room temperature is attributed to the nanoscale crystallite size that allows modulation of depletion layer across the grains to be completely modulated by the gas adsorption of $NO_2$ [16]. The electrostatic stabilization of defect states attributed to microstrain, in turn, promote charge transfer and adsorption [17]. Higher molecular kinetic speed induced desorption at high temperature will reduce the recovery time [18]. Clearly the sensing dynamics depend upon the balance between depletion effects due to finite grain size and the adsorption-desorption kinetics that depend on temperature.

Figure (10) illustrates the variation of sensitivity toward 75 ppm $NO_2$ at different operating temperatures. The highest sensitivity was recorded at room temperature (25°C), followed by a decrease at 100°C and 200°C. The enhanced room-temperature sensitivity is primarily attributed to the nanoscale crystallite size (14.14 nm), which allows the depletion region induced by $NO_2$ adsorption to extend across a significant portion of the grain volume, leading to pronounced resistance modulation [19].

From a physical perspective, this behavior can be understood in terms of the Debye length ($L_D$), which represents the thickness of the surface depletion layer in semiconductor materials. In oxide semiconductors, $L_D$ is typically in the nanometer range. When the crystallite size becomes comparable to twice the Debye length ($D \lesssim 2L_D$), the depletion region can extend throughout most of the grain volume, and the volume depletion model becomes applicable, resulting in enhanced sensitivity.

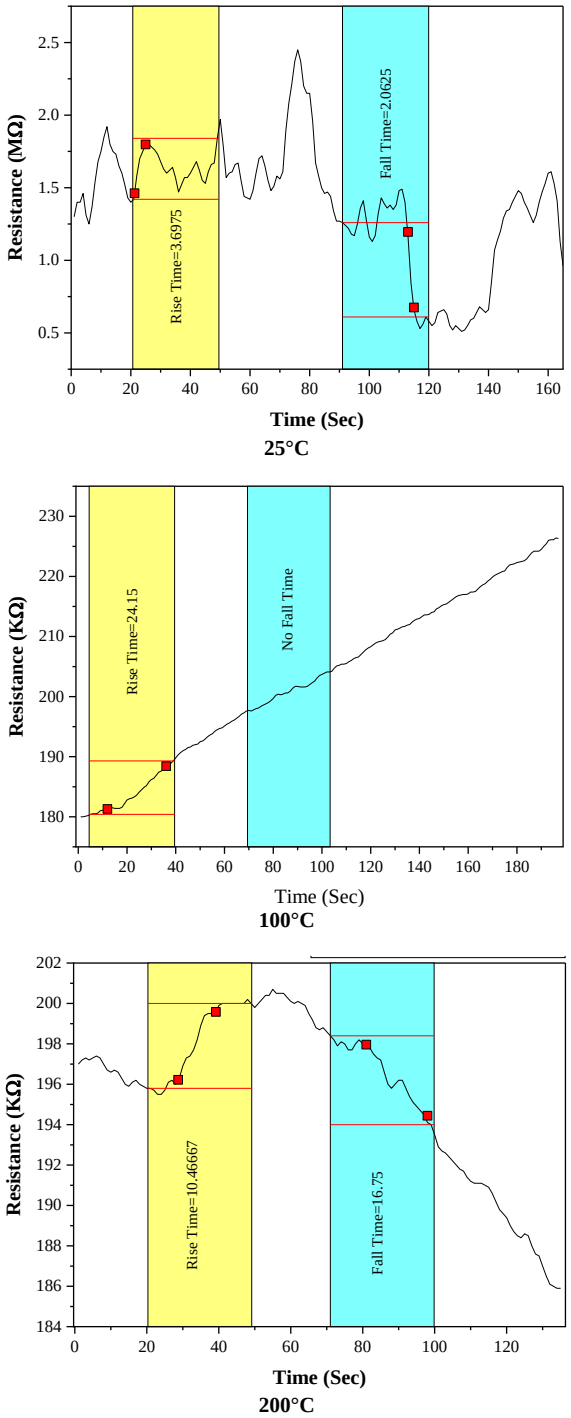


**Fig. (8) Response of the multilayer ZnO:$SnO_2$:CdS/p-Si structure deposited on silicon to $NO_2$ under different operating temperatures (25°C, 100°C, and 200°C)**

In addition, the relatively high microstrain ($3.14\times10^{-3}$) indicates increased defect density, which provides abundant active adsorption sites and enhances electron withdrawal from the n-type layers upon exposure to oxidizing $NO_2$ gas [20]. At higher temperatures, thermally activated desorption becomes more dominant and decreases the steady-state surface charge density, limiting depletion layer expansion.

  

Thus, although molecular mobility is enhanced, the sensitivity decreases [21]. In addition, the increase in intrinsic carrier concentration at higher temperatures leads to a reduction in baseline resistance, which decreases the relative resistance change (ΔR/R) and consequently lowers the signal-to-noise ratio.

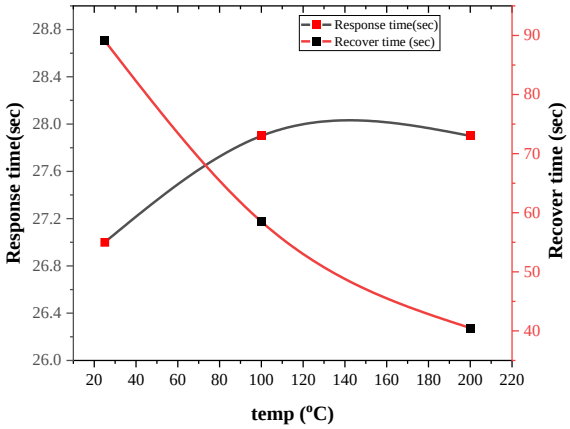


**Fig. (9) Response and recovery times when exposed to $NO_2$ gas under different operating temperatures**

The exceptional room-temperature sensing performance is attributed to the effective multilayer heterostructure and defect-assisted charge modulation, highlighting that nanoscale structural control plays a key role in improving gas sensing performance.

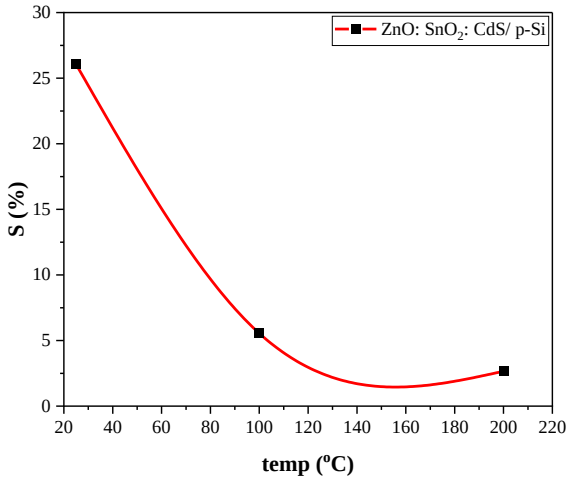


**Fig. (10) Sensitivity of the multilayer thin film structure when exposed to $NO_2$ gas under different operating temperatures**

## 4. Conclusion

Driven by nanoscale crystallinity and interfacial coupling effects, the effective $NO_2$ sensing behavior of the ZnO/$SnO_2$/CdS multi-heterojunction deposited on p-type silicon. These smaller crystallite sizes and higher microstrain correlate with increased active sites for adsorption, as well as effective depletion layer modulation between heterointerface. The room temperature charge transfer and resistance variation would benefit from the synergistic interaction of wide band gap oxides (ZnO, $SnO_2$) and the narrower band gap CdS layer. The best sensing performance achieved at 25 °C indicates that the structural factors are the most important for facilitating efficient surface charge tuning without a need for thermal activation from the nano-to microscale in temperatures away from room temperature. The decrease in sensitivity with increasing temperature is a demonstration of the kinetic effect of adsorption-desorption rules over defect assisted charge trapping the defect becomes less critical as temperature increases. This leads us to conclude that multilayer architecture engineering, as well as defect density control, is imperative for optimizing low-temperature metal-oxide gas sensors specifically for the gas of interest, here $NO_2$ something that is not easy to achieve in real-life applications.

## References

[1] M.I. Ibrahim et al., "Latest developments in $NO_2$ gas sensors based on PEDOT: PSS nanocomposites and metal oxides: A comprehensive review", *NTU J. Renew. Ener.*, 10(1) (2026) 11-20.

[2] M.W. Alam et al., "The recent development in chemoresistive-based heterostructure gas sensor technology, their future opportunities and challenges: A review", *Membranes*, 12(6) (2022) 555.

[3] I.K. Er et al., "ZnO/$SnO_2$ based composite heterostructure for $NO_2$ gas sensing properties", *Ceram. Int.*, 51(1) (2025) 623-635.

[4] S. Wang et al., "Enhancing $NO_2$ sensing performance through interface engineering in $Cs_2AgBiBr_6$/$SnO_2$/ZnO-NRs sensor", *Sens. Actuat. B: Chem.*, 422 (2025) 136654.

[5] V.V. Petrov et al., "High gas sensitivity to nitrogen dioxide of nanocomposite ZnO-$SnO_2$ films activated by a surface electric field", *Nanomater.*, 12(12) (2022) 2025.

[6] H. Chen et al., "Gas sensors based on semiconductor metal oxides fabricated by electrospinning: a review", *Sensors*, 24(10) (2024) 2962.

[7] M. Heikkinen, R. Ghiyasi and M. Karppinen, "Layer-engineered functional multilayer thin-film structures and interfaces through atomic and molecular layer deposition", *Adv. Mater. Interfaces*, 12(4) (2025) 2400262.

[8] A. Ashok et al., "Comparative studies of CdS thin films by chemical bath deposition techniques as a buffer layer for solar cell applications", *J. Mater. Sci.: Mater. Electron.*, 31(10) (2020) 7499-7518.

[9] K. Qi et al., "High-detectivity solar-blind deep UV photodetectors based on cubic/monoclinic mixed-phase $(In_xGa_{1-x})_2O_3$ thin films", *J. Alloys Comp.*, 965 (2023) 171473.

[10] M.I. Hossain et al., "Exploring the optical and morphological properties of metal oxide thin films produced via reactive electron beam

  

evaporation", *Cogent Eng.*, 11(1) (2024) 2338144.
[11] X. Zhao et al., "Interface engineering in 1D ZnO-based heterostructures for photoelectrical devices", *Adv. Func. Mater.*, 32(11) (2022) 2106887.
[12] W. Mönch, "Valence-band offsets and Schottky barrier heights of layered semiconductors explained by interface-induced gap states", *Appl. Phys. Lett.*, 72(15) (1998) 1899-1901.
[13] P. Sarangapani et al., "Band-tail formation and band-gap narrowing driven by polar optical phonons and charged impurities in atomically resolved III-V semiconductors and nanodevices", *Phys. Rev. Appl*., 12(4) (2019) 044045.
[14] Z. Zhang et al., "Recent advances in functionalizing metal oxide semiconductors for highly sensitive gas sensors", *Small Methods*, 9(10) (2025) 2500228.
[15] J.H. Yue et al., "Synthesis and calcination–temperature-dependent gas-sensing performance of g-$C_3N_4$/$Co_3O_4$ heterojunctions for toluene gas sensors", *J. Mater. Sci.: Mater. Electron.*, 34(21) (2023) 1572.
[16] H. Chen et al., "Gas sensors based on semiconductor metal oxides fabricated by electrospinning: a review", *Sensors*, 24(10) (2024) 2962.
[17] X. Yang et al., "Functionalization of mesoporous semiconductor metal oxides for gas sensing: Recent advances and emerging challenges", *Adv. Sci.*, 10(1) (2023) 2204810.
[18] M.K. Sahu et al., "Development and Synthesis Methodology of Versatile Bulk and Nanostructured Material for Gas Sensors", in **Advancement in Gas Sensors: Self-Powered Innovations for Real-World Impact**, Cham:Springer Nature (Switzerland, 2025), pp. 107-138.
[19] H. Chai et al., "Stability of metal oxide semiconductor gas sensors: A review", *IEEE Sens. J.*, 22(6) (2022) 5470-5481.
[20] W. Ding et al., "Oxygen defects in nanostructured metal-oxide gas sensors: recent advances and challenges", *Chinese J. Chem.*, 38(12) (2020) 1832-1846.
[21] P.K. Panigrahi, B. Chandu and N. Puvvada, "Recent advances in nanostructured materials for application as gas sensors", *ACS Omega*, 9(3) (2024) 3092-3122.

  